Electronic Supplementary Information (ESI)

Heat-triggered high-performance thermocells enable self-powered forest fire alarming

Boyang Yu, Wei Yang, Jia Li, Wenke Xie, Hongrun Jin, Rong Liu, Hui Wang, Xinyan Zhuang, Bei Qi, Shiyou Liu, Liang Huang, Bin Hu, Jiangjiang Duan* and Jun Zhou*

Wuhan National Laboratory for Optoelectronics, Huazhong University of Science and Technology, Wuhan 430074, China.
*Correspondence to: jiangjduan@hust.edu.cn and jun.zhou@mail.hust.edu.cn

This PDF file includes:

Other Supplementary Information for this manuscript include the following:

Videos S1 to S4

Supplementary Note 1. Theoretical analysis of the thermocell

For a thermocell (TC) using $Fe(CN)_6^{3-}/Fe(CN)_6^{4-}$ aqueous electrolyte ($Fe(CN)_6^{3-} + e^- \leftrightarrow Fe(CN)_6^{4-}$), a potential difference (ΔE) can be generated between two electrodes by applied a temperature difference (ΔT), due to the dependence electrical redox potential (E) on temperature (generally named thermopower for the TC).[1,2] According to the Nernst equation, the electrical redox potential (E) of the abovementioned redox reaction can be expressed as:

$$E = E^0 + \frac{RT}{F}\ln\frac{(\alpha_{Fe(CN)_6^{3-}})}{(\alpha_{Fe(CN)_6^{4-}})} \tag{S1}$$

where E^0 is the standard potential, α is the activity of redox specie, R is the ideal gas constant, and F is Faraday's constant. The activity (α) is defined as the product of the activity coefficient (γ) and concentration (c) ($\alpha=\gamma\times c$). Thus, Eq. (S1) can be expressed as:

$$E = E^0 + \frac{RT}{F}\left[\ln\frac{(\gamma_{Fe(CN)_6^{3-}})}{(\gamma_{Fe(CN)_6^{4-}})} + \ln\frac{(c_{Fe(CN)_6^{3-}})}{(c_{Fe(CN)_6^{4-}})}\right] \tag{S2}$$

The open-circuit voltage (V_{oc}) of TC is generated by the difference of E for the cold (E_{cold}) and the hot sides (E_{hot}), and thereby can be calculated by:

$$V_{oc} = \frac{R}{F}\left[T_{cold}\ln\frac{(\gamma_{Fe(CN)_6^{3-}})_{cold}}{(\gamma_{Fe(CN)_6^{4-}})_{cold}} + T_{hot}\ln\frac{(\gamma_{Fe(CN)_6^{4-}})_{hot}}{(\gamma_{Fe(CN)_6^{3-}})_{hot}}\right] + \frac{R}{F}\left[T_{cold}\ln\frac{(c_{Fe(CN)_6^{3-}})_{cold}}{(c_{Fe(CN)_6^{4-}})_{cold}} + T_{hot}\ln\frac{(c_{F}\right. \tag{S3}$$

whereas the first term containing the activity coefficient (γ) is considered to be dominated by the solvent-dependent difference in entropy between the redox species, the second term is only related to the concentration ratio of the redox species.[3,4] Here, we define the solvent-dependent entropy difference (ΔS) and the concentration ratio difference (ΔC) as:

$$\Delta S = \left[T_{cold} \ln \frac{(\gamma_{Fe(CN)_6^{3-}})_{cold}}{(\gamma_{Fe(CN)_6^{4-}})_{cold}} + T_{hot} \ln \frac{(\gamma_{Fe(CN)_6^{4-}})_{hot}}{(\gamma_{Fe(CN)_6^{3-}})_{hot}} \right] \times \frac{R}{\Delta T} \quad \text{(S4)}$$

$$\Delta C = \left[T_{cold} \ln \frac{(c_{Fe(CN)_6^{3-}})_{cold}}{(c_{Fe(CN)_6^{4-}})_{cold}} + T_{hot} \ln \frac{(c_{Fe(CN)_6^{4-}})_{hot}}{(c_{Fe(CN)_6^{3-}})_{hot}} \right] \times \frac{R}{\Delta T} \quad \text{(S5)}$$

Therefore, the Eq. (S3) can be simplified as:

$$V_{oc} = \frac{(\Delta S + \Delta C)}{F} \times \Delta T \quad \text{(S6)}$$

For the typical equal-concentration $Fe(CN)_6^{3-}/Fe(CN)_6^{4-}$ system (TC), both the concentration ratios of $Fe(CN)_6^{3-}$and $Fe(CN)_6^{4-}$ on the hot and the cold sides equal 1 under open-circuit state, obviously causing ΔC=0. Therefore, the V_{oc} of such TC is only distributed by ΔS:

$$V_{oc} = \frac{\Delta S}{F} \times \Delta T \quad \text{(S7)}$$

And the V_{oc} also can be calculated by the product of thermopower and ΔT.[5,6] Early studies consistently showed that the thermopower slightly depended on the concentration of $Fe(CN)_6^{3-}/Fe(CN)_6^{4-}$, nearly a constant ~1.4 mV K^{-1}.[7,8] Such result is also proven by our measured V_{oc} profile of a pristine TC (Fig. 1b).

By approximately using thermopower of 1.4 mV K^{-1}, Eq. (S3) can be further written as:

$$V_{oc} = \left(1.4 + \frac{\Delta C}{F}\right) \times \Delta T \quad \text{(S8)}$$

Remarkably, the V_{oc} of TC can be highly boosted by simultaneously introducing the concentration gradients of $Fe(CN)_6^{3-}/Fe(CN)_6^{4-}$ on the cold side ($Fe(CN)_6^{3-}$>>$Fe(CN)_6^{4-}$) and the hot side ($Fe(CN)_6^{4-}$>>$Fe(CN)_6^{3-}$). Here, we named such a hypothetical TC as concentration gradient-boosted thermocell (TCC) and the contribution of concentration gradients as CG (the second term of Eq. (S8)). Based on Eq. (S8), we simulated the V_{oc} of a TCC with both the concentration ratios of $Fe(CN)_6^{3-}/Fe(CN)_6^{4-}$ on the cold side and $Fe(CN)_6^{4-}/Fe(CN)_6^{3-}$ on the hot side set as 1000 (Fig. 1b and Fig. S1).

Supplementary Figures

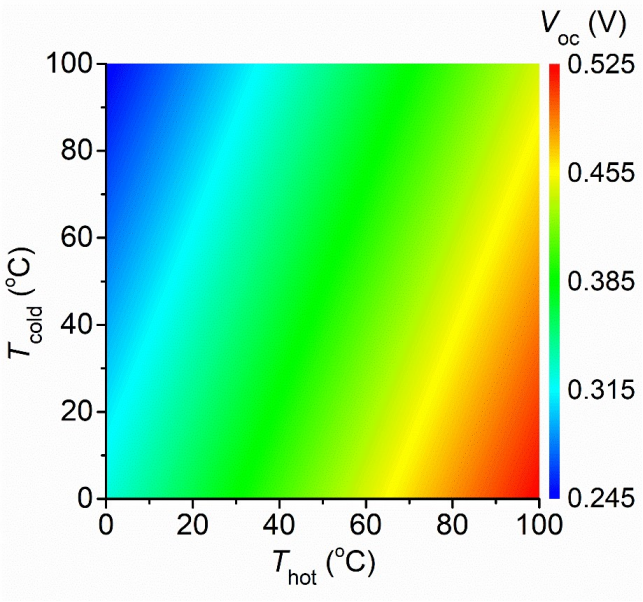

Figure S1. Simulated V_{oc} of the TCC depending on the temperature of the cold and the hot electrodes. Both the concentration ratios of $Fe(CN)_6^{4-}/Fe(CN)_6^{3-}$ on the hot side and $Fe(CN)_6^{3-}/Fe(CN)_6^{4-}$ on the cold side were preset as 1000. The simulation is based on theoretical analysis (Supplementary Note 1).

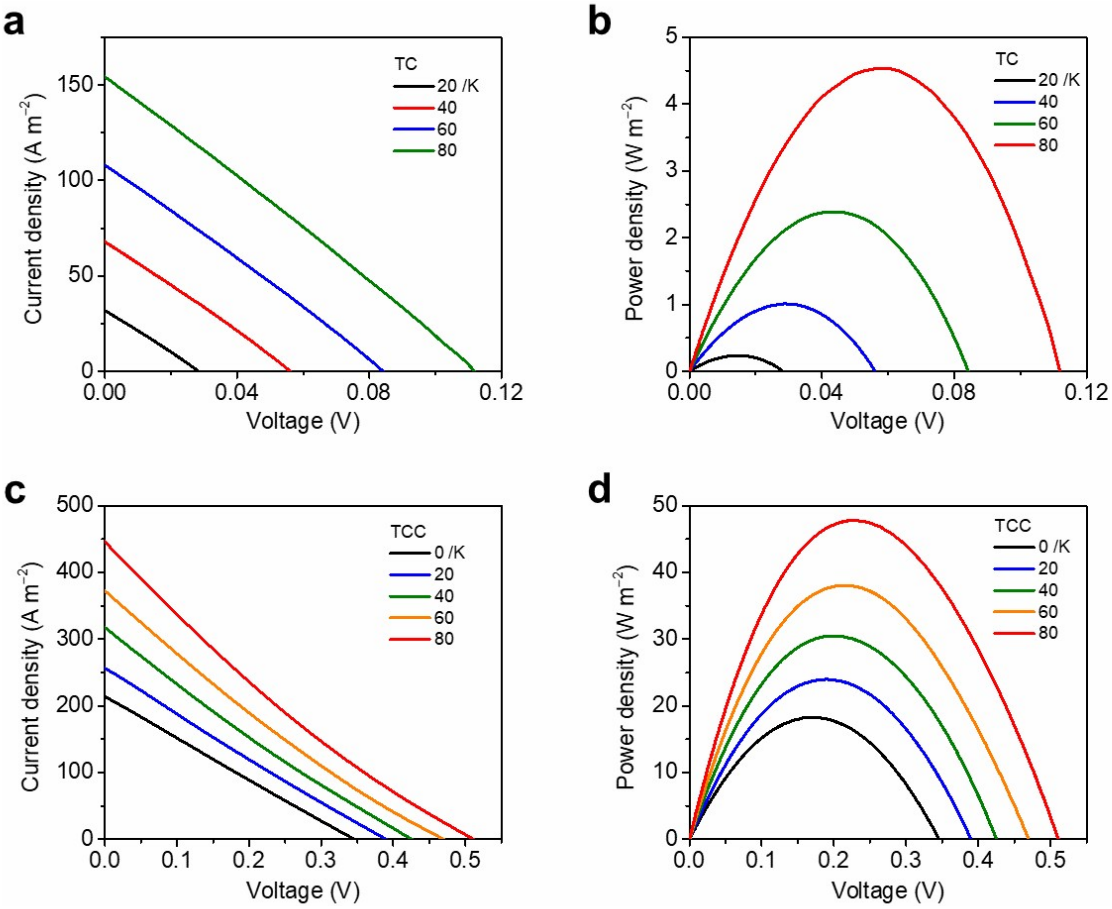

Figure S2. (a, c) Current–voltage curves for the TC and TCC at different ΔT, and their corresponding power densities (b, d). The output of TCC at a ΔT of 0 K is totally contributed by the introduced concentration gradients.

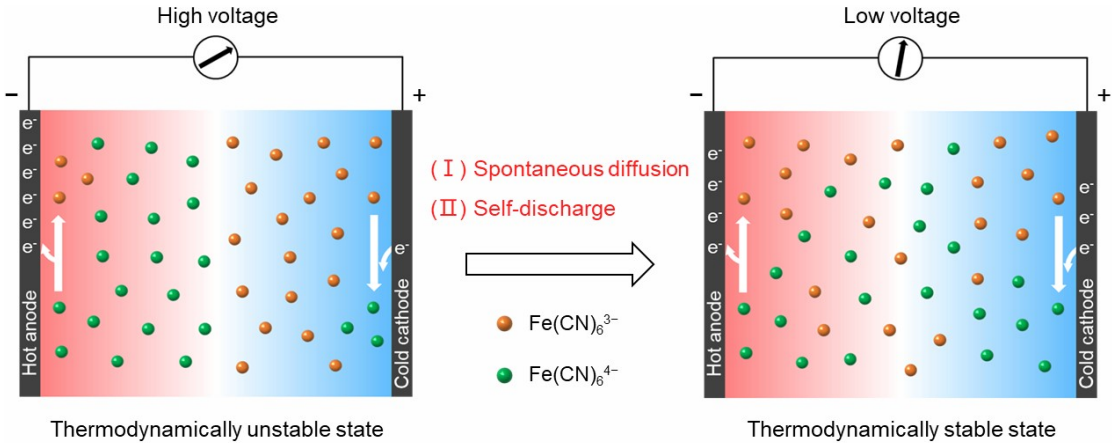

Figure S3. Schematic of the TC boosted by a transient concentration gradient (left), which is thermodynamically unstable and will spontaneously decay into a homogeneous and thermodynamically stable state (right).

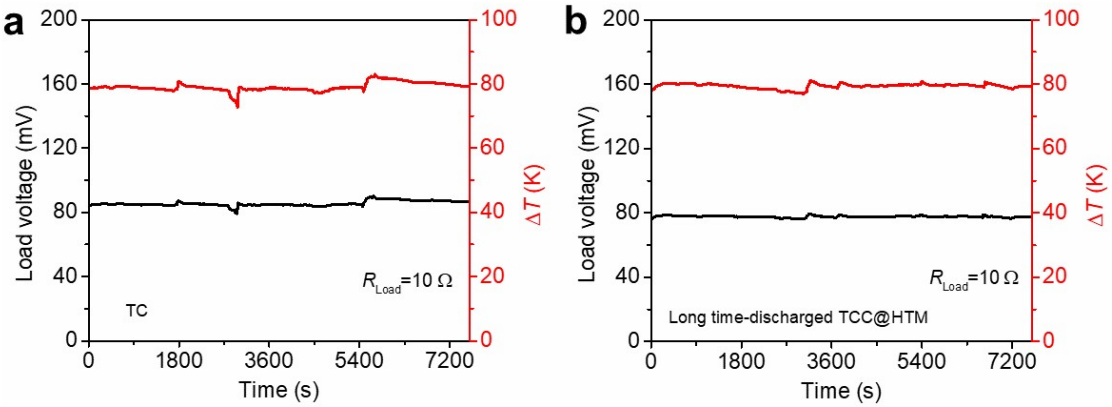

Figure S4. Continuous operations of the pristine TC (a) and the long time-discharged TCC (b), discharged with a 10 Ω load resistance at a ΔT of ~80 K. The cold side temperature was controlled at ~291 K. Here, the "long time-discharged TCC@HTM" represents a TCC in which the concentration gradients have been totally decayed by discharging and a HTM have been used.

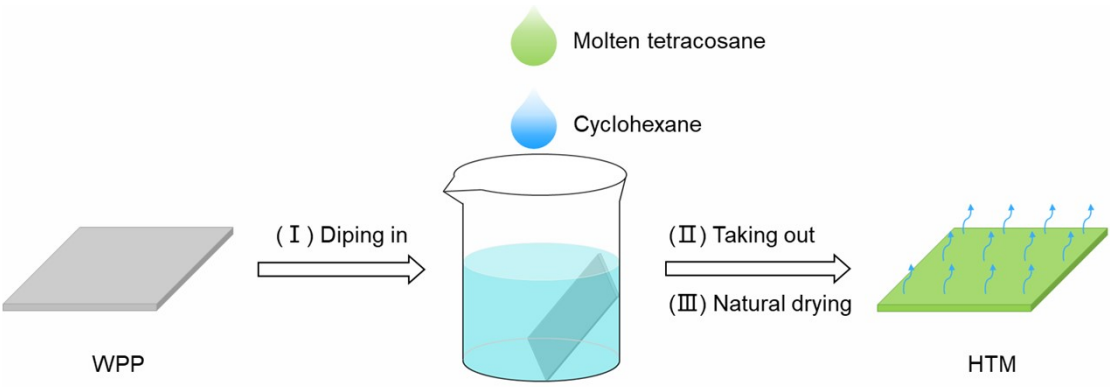

Figure S5. Schematic of the process of preparing the heat-triggered membrane (HTM).

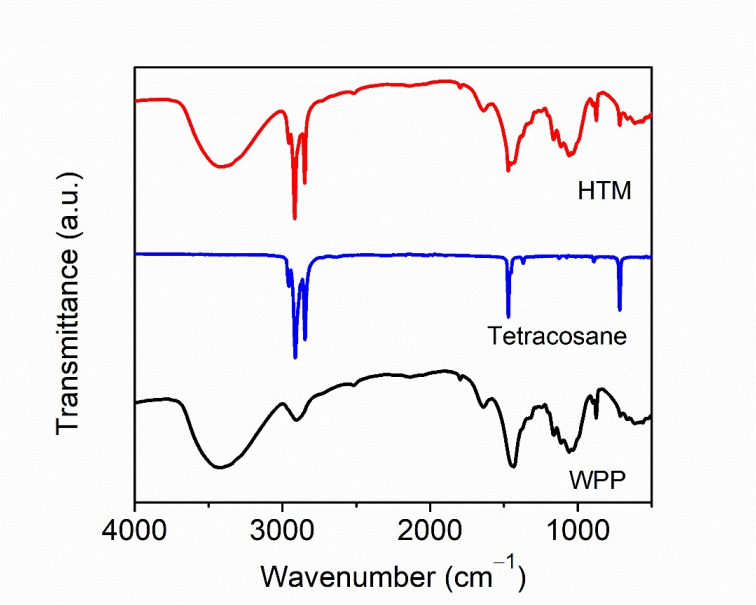

Figure S6. FTIR spectra of the HTM composed of the tetracosane and the wood pulp paper (WPP).

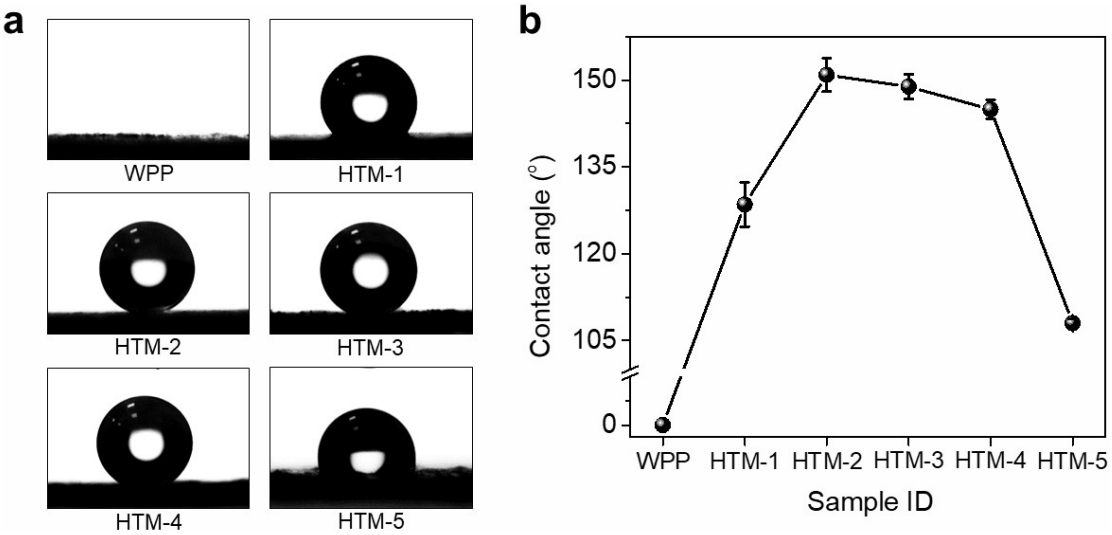

Figure S7. (a) Photographs of water drops on the WPP and various HTM samples. (b) Contact angles of the WPP and various HTM samples. Each point is a statistic from five different samples.

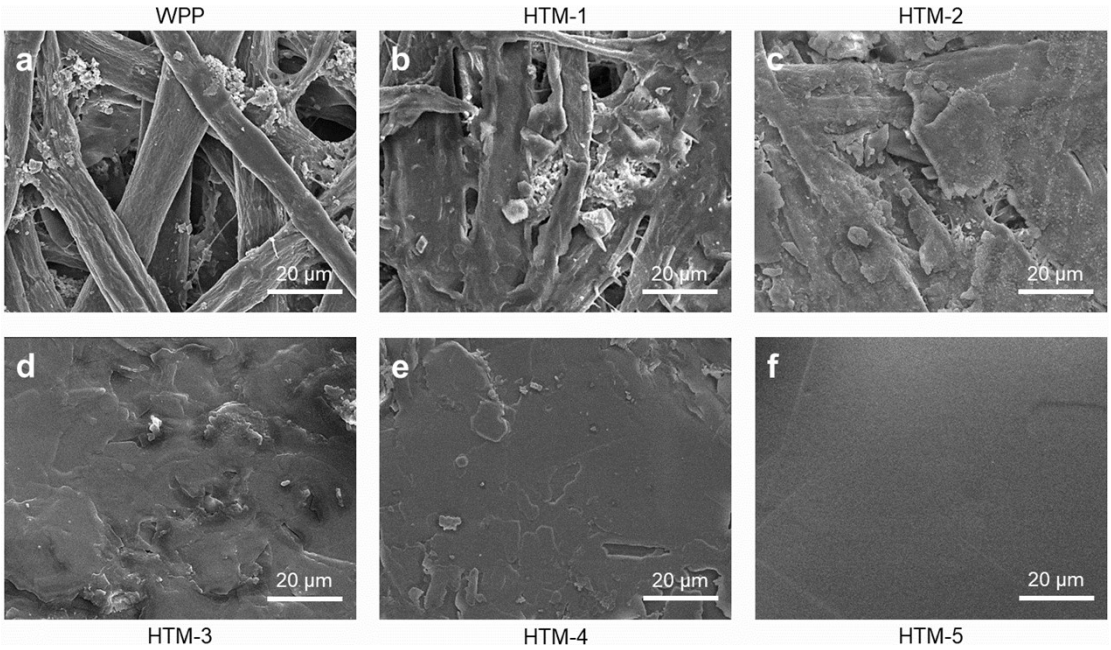

Figure S8. SEM images of the WPP and various HTM samples.

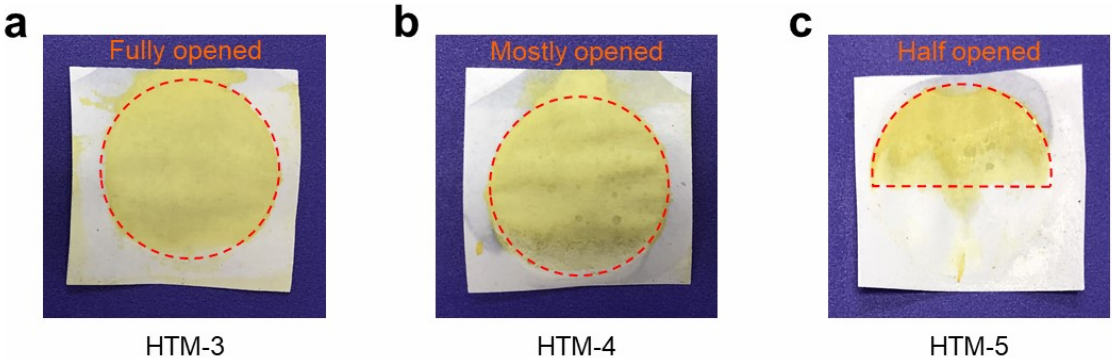

Figure S9. Photographs of various HTM samples after the heat-triggered test in Fig. 3d.

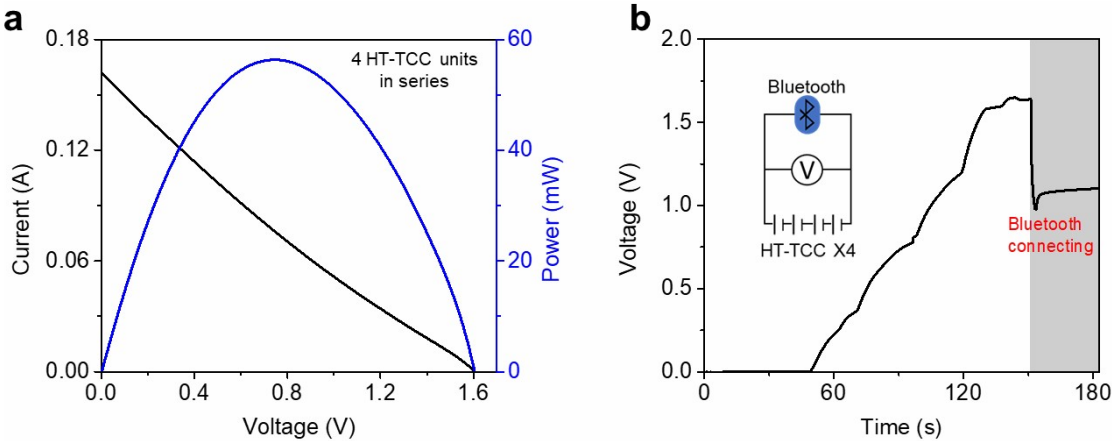

Figure S10. (a) Current-voltage curve (black) and corresponding power output (blue) of a HT-TCC module integrated by 4 units in series. The established ΔT across the module was ~35 K. (b) Real-time voltage curve of the module tested in the simulated precombustion for driving a commercial Bluetooth to connect a mobile phone. The inset shows the operated circuit diagram.

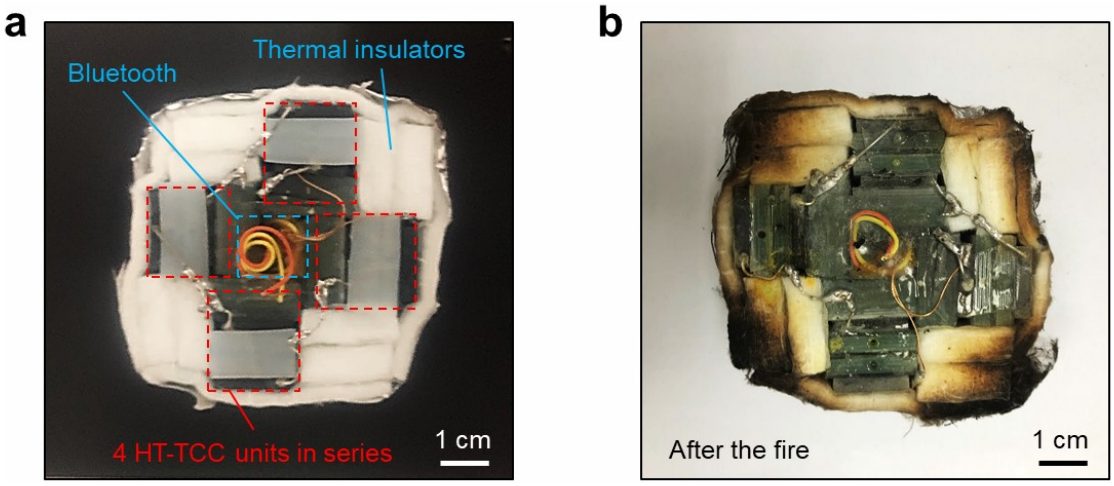

Figure S11. (a) Photograph of a prototype device for fire detection and alarm, containing a cube-shaped HT-TCC module and a Bluetooth. (b) Photograph of the device after the open fire test.

Supplementary Table

Table S1. Sample ID of HTM and corresponding volume ratio of tetracosane and cyclohexane used in preparation.

Simple ID	Volume ratio of tetracosane and cyclohexane (x:y)
HTM-1	1:20
HTM-2	1:10
HTM-3	1:5
HTM-4	1:3
HTM-5	1:0

Captions for Videos S1 to S4

Video S1. Dynamic contact angle test of the HTM with heating off and on.

Video S2. Dyeing test of the HTM with heating off and on.

Video S3. Demonstration of the HT-TCC module for the precombustion detection and alarm.

Video S4. Demonstration of the prototype device for the open fire detection and alarm.

Supplementary References

1. T. I. Quickenden and Y. Mua, *J. Electrochem. Soc.*, 1995, **142**, 3985-3994.
2. M. F. Dupont, D. R. MacFarlane and J. M. Pringle, *Chem. Commun.*, 2017, **53**, 6288-6302.
3. B. Yu, J. Duan, H. Cong, W. Xie, R. Liu, X. Zhuang, H. Wang, B. Qi, M. Xu, Z. L. Wang and J. Zhou, *Science*, 2020, **370**, 342-346.
4. T. Kim, J. S. Lee, G. Lee, H. Yoon, J. Yoon, T. J. Kang and Y. H. Kim, *Nano Energy*, 2017, **31**, 160-167.
5. J. Duan, G. Feng, B. Yu, J. Li, M. Chen, P. Yang, J. Feng, K. Liu and J. Zhou, *Nat. Commun.*, 2018, **9**, 5146.
6. H. Zhou, T. Yamada and N. Kimizuka, *J. Am. Chem. Soc.*, 2016, **138**, 10502-10507.
7. T. J. Kang, S. Fang, M. E. Kozlov, C. S. Haines, N. Li, Y. H. Kim, Y. Chen and R. H. Baughman, *Adv. Funct. Mater.*, 2012, **22**, 477-489.
8. J. H. Kim, J. H. Lee, R. R. Palem, M.-S. Suh, H. H. Lee and T. J. Kang, *Sci. Rep.*, 2019, **9**, 8706.